Journal of Inorganic Biochemistry 137 (2014) 1–11

Contents lists available at ScienceDirect

Journal of Inorganic Biochemistry

journal homepage: www.elsevier.com/locate/jinorgbio

Synthesis, characterization, crystal structures and biological activity of set of Cu(II) benzothiazole complexes: Artificial nucleases with cytotoxic activities

Ramsey A. Steiner [a], David Foreman [a], Han X. Lin [a], Bruce K. Carney [b], Kristin M. Fox [a], Lynne Cassimeris [b], Joseph M. Tanski [c], Laurie A. Tyler [a,*]

[a] Department of Chemistry and Biochemistry, Union College, Schenectady, NY 12308, United States
[b] Department of Biological Sciences, Lehigh University, Bethlehem, PA 18015, United States
[c] Department of Chemistry, Vassar College, Poughkeepsie, NY 12604, United States

ARTICLE INFO

Article history:
Received 22 January 2014
Received in revised form 1 April 2014
Accepted 2 April 2014
Available online 12 April 2014

Keywords:
Benzothiazole
Quinoline
Copper(II)
Protonated phenol
Nuclease

ABSTRACT

A series of Cu(II) complexes with ligand frames based on quinoline derivatives appended with a benzothiazole substituent has been isolated. The complexes, $Cu(Q(oBt))(NO_3)_2(H_2O)\cdot CH_3OH$ (**1** · CH_3OH), $Cu(8OHQ(oBt))Cl_2 \cdot CH_3OH$ (**2** · CH_3OH), $Cu(8OQ(oBt))Cl(CH_3OH)\cdot CH_3OH$ (**3** · CH_3OH) and $[Cu(8OH_{1/2}Q(oBt))(CH_3OH)(NO_3)]_2(NO_3)$ (**4**) have been characterized by single crystal X-ray diffraction, IR and UV-visible spectroscopies, and elemental analysis. The ligand frame within the set of complexes differs in the substituent on the quinoline ring: complex **1** remains unsubstituted at this position while complexes **2**–**4** have a substituted −OH group. In complex **2**, the bound phenol remains protonated while in **3** it is a phenolato group. Complex **4** contains two complexes within the unit cell and one NO_3^- giving rise to an overall 'half-protonation'. The interaction between complexes **1**–**3** with CT-DNA was investigated using fluorescence emission spectroscopy and revealed **2** and **3** strongly intercalate DNA with K_{app} values of $1.47 \times 10^7\ M^{-1}$ and $3.09 \times 10^7\ M^{-1}$, respectively. The ability of complexes **1**–**3** to cleave SC-DNA was monitored using gel electrophoresis. Each complex exhibits potent, concentration dependent nuclease activity forming single and double-nicked DNA as low as 10 μM. The nuclease activity of complexes **1**–**3** is primarily dependent on $^1O_2$ species while ·OH radicals play a secondary role in the cleavage by complexes **2** and **3**. The cytotoxic effects of **1**–**3** were examined using HeLa cells and show cell death in the micromolar range. The distribution of cell cycle stages remains unchanged when complexes are present indicating DNA damage may be occurring throughout the cell cycle.

1. Introduction

Platinum based chemotherapeutics such as cisplatin, carboplatin and oxaliplatin have been extremely useful in cancer treatment. Indeed, after the FDA approved cisplatin in 1978, the cure rate for testicular cancer improved to nearly 90% with early detection [1]. The mechanism of action for these platinum based drugs has been extensively studied and found to rely on the coordinate covalent bonds that form between the platinum metal center and the nitrogen atoms of the nucleic acid backbone in DNA. Due to the strong Pt-N_{DNA} bond, cellular DNA repair mechanisms fail and programmed cell death occurs [2]. These platinum based drugs have been instrumental in treating a subset of cancers; however they are not effective against all types. Additionally, there are drawbacks to platinum based chemotherapy including severe side effects associated with acute and cumulative toxicity as well as acquired resistance due to heavy metal detoxification mechanisms [3].

Over the last decade there has been increased interest in the development of new non-platinum based metallo-chemotherapeutics to meet the need of treating a broader range of cancer strains with decreased side effects. The use of copper in this endeavor is attractive from several standpoints and includes the diverse reactivity of the metal center, due in part to the accessibility of the Cu(II)/Cu(I) redox couple, along with the bioessentiality of the metal; copper is involved in vital life processes including DNA synthesis, energy metabolism and respiration, all of which rely on well-developed biological transport mechanisms for the metal [4,5]. Additionally, a positive correlation between serum copper concentration and tumor incidence, stage of the diseases and mass of the growth in a variety of cancers (including leukemia, breast and liver, among others) has been reported and it is known that copper is essential for the tumor angiogenesis processes [6,7]. Overall, the biological relevance of copper may lead to tumor specific copper chemotherapeutics [8–11].

Small molecule copper complexes have been shown to interact with DNA via electrostatic interactions or by intercalating directly between the nucleic acids. Some copper complexes also have the ability to act as

* Corresponding author. Tel.: +1 518 388 7123; fax: +1 518 388 6795.
E-mail address: tylerl@union.edu (L.A. Tyler).

http://dx.doi.org/10.1016/j.jinorgbio.2014.04.002
0162-0134/

nucleases, initiating both single and double strand cleavage via hydrolytic or oxidative pathways [12–15]. Research efforts in this area have shown that the nuclease ability as well as the cytotoxic activity of the complexes is highly dependent on the organic ligand frame around the copper [4,16–21]. Indeed, structural features and donor atoms of the complex can influence important factors such as the lipophilic/hydrophilic nature of the compound, the favored oxidation state of the copper center, as well as the observed biological reactivity of the complex [5]. Although some general correlations have been found, none extend to all small molecule copper species, making a case by case approach useful toward elucidating aspects of structure–function relationships as it pertains to the biological activity of small molecule copper complexes. Therefore efforts toward the design, synthesis and characterization of new copper compounds for use as potential antitumor agents remain an important area of research. It has been suggested that over 10,000 complexes need to be evaluated to obtain one new successful anticancer drug [2,22].

In this work we have isolated a series of Cu(II) complexes with ligand frames based on derivatives of a quinoline group appended

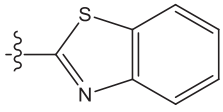

Benzothiazole (oBt)

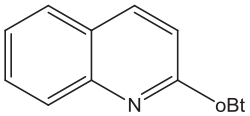

Q(oBt)

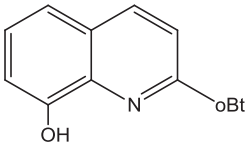

8OHQ(oBt)

with a benzothiazole substituent.

Organic moieties containing the quinoline structure are known to be biologically active and are widely used as anti-bacterial and malarial drugs [23–29]. The step-wise modification of this motif further elucidates how structural changes in the ligand frame modulate the observed reactivity. Likewise, the biological applications of the benzothiazole moiety have not been well investigated even though the thiazole group is a key component in thiamin, an essential bio-nutrient involved in carbohydrate metabolism [30,31]. Furthermore, the corresponding benzimidazole group has been reported to possess a wide range of biological activities including anticancer, antioxidant and antiviral activities [32–34]. Consideration of these facts indicates that metal complexes containing these structures within the ligand frame could be of great interest.

Here we present the syntheses, spectroscopic characterizations, and X-ray crystal structures of four complexes, $Cu(Q(oBt))(NO_3)_2(H_2O)$ (**1**), $Cu(8OHQ(oBt))Cl_2$ (**2**), $Cu(8OQ(oBt))Cl(CH_3OH)\cdot CH_3OH$ (**3** · CH_3OH), and $[Cu(8OH_{1/2}Q(oBt))(CH_3OH)(NO_3)]_2(NO_3)$ (**4**) and have evaluated biological activities of complexes **1**–**3** including nuclease activity and DNA binding. Additionally, the in vitro cytotoxicity activity of complexes **1**–**3** on human HeLa cells is reported.

2. Experimental

2.1. Materials and methods

All reagents and solvents were purchased commercially and used as received unless otherwise noted. Calf thymus DNA (CT-DNA), ascorbic acid, L-histidine, and ethidium bromide (EtBr) were purchased from Sigma-Aldrich. Agarose (molecular biology grade) was purchased from Fisher Scientific and 6× loading dye and DNA ladder were purchased from Promega Corporation. Incubation buffer (5 mM Tris [tris(hydroxymethyl)-aminomethane]/50 mM NaCl, pH 7.2), was prepared by adjusting the pH of the Tris/NaCl solution with 1 M NaOH. Gel running buffer (40 mM Tris, 1 mM EDTA), pH 8.3 was prepared by adjusting the pH with glacial acetic acid. Supercoiled DNA (SC-DNA) was prepared via plasmid mini-preps of pGEM plasmid DNA (Promega) circularized with a 1 kb insert. CT-DNA was prepared by dissolving a small amount of DNA in several mL of 5 mM Tris/50 mM NaCl, pH 7.2 in a 15 mL polypropylene conical centrifuge tube (Fisher) and sonicating the contents until the CT-DNA was dissolved. The concentrations of nucleic acid in the SC-DNA and CT-DNA solutions was determined by UV/Vis spectroscopy using $\varepsilon_{258} = 0.02\ (\mu g/mL)^{-1}\ cm^{-1}$.

HeLa, a human cancer cell line, was obtained from the ATCC (Manassas, Virginia). HeLa cells were cultured in DMEM (Life Technologies, Rockville, MD), supplemented with 10% fetal bovine serum (FBS; Invitrogen) and an antibiotic/antimycotic solution (Sigma). Cells were grown at 37 °C in a 5% CO_2 atmosphere.

2.2. Instrumentation

Infrared spectra were obtained with a Thermoelectron, Avatar 330 FT-IR spectrophotometer equipped with a Smart Orbit reflectance insert, diamond window. Absorption spectra were measured on a Hewlett-Packard 8453 diode array spectrophotometer. ^1H NMR spectra were recorded on a Bruker 400 MHz spectrometer. Fluorescence emission spectra were measured with a Photon Technology QuantaMaster spectrometer. Agarose gel electrophoresis of plasmid DNA cleavage experiments were performed using an Owl Easy Cast System (ThermoScientific). Bands were visualized and imaged using a G:Box (Syngene). The gels were analyzed using the Gene Tools program (Syngene), version 3.06.04.

2.3. Preparation of ligands and compounds

2.3.1. Synthesis of 2-quinolinebenzothiazole (Q(oBt))

A batch of 2-quinoline carboxaldehyde (501 mg, 3.19 mmol) was dissolved in ~20 mL ethanol (EtOH) and 340 μL of o-aminobenzenethiol (ABT) (3.19 mmol) were added. The solution was refluxed for 1 h. The solvent was then reduced to ~10 mL and the resultant light brown solid was collected, washed with 5 mL of hexanes, and then dried under vacuum. Yield: 480 mg (57%). If any benzothiazoline was present after analysis, the solid was dissolved in $CHCl_3$ and refluxed in air for an additional 2–4 h. ^1H NMR ($CDCl_3$, 400 MHz, 25 ° C, δ from tetramethylsilane (TMS)): 8.53 (d, 1H), 8.33 (d, 1H), 8.23 (d, 1H), 8.17 (d, 1H), 8.02 (d, 1H), 7.90 (d, 1H), 7.80 (t, 1H), 7.63 (t, 1H), 7.56 (t, 1H), 7.48 (t, 1H). Selected IR bands: (cm^{-1}) 1591 ($\nu_{N=C}$), 1499 (m), 750 (s).

2.3.2. Synthesis of 2-(benzothiazole)8-hydroxyquinoline (8OHQ(oBt))

A batch of 8-hydroxy-2-quinoline carboxaldehyde (250 mg, 1.44 mmol) was dissolved in 25 mL of EtOH and 154 μL of ABT (1.44 mmol) was added. The solution was refluxed for 1 h, the solvent was reduced to ~10 mL, and the resulting yellow solid was collected, washed with 5 mL of hexanes and dried under vacuum. Yield: 284 mg (71%). If any benzothiazoline was present after analysis, the solid was dissolved in $CHCl_3$ and refluxed in air for 2–4 h. ^1H NMR ($CDCl_3$, 400 MHz, 25 °C, δ from TMS): 8.55 (d, 1H), 8.34 (d, 1H), 8.17 (d, 1H), 8.09 (s, 1H), 8.02 (d, 1H), 7.49 (m, 5H). Selected IR bands: (cm^{-1}) 3410 (ν_{OH}), 1566 ($\nu_{N=C}$), 1456 (s), 1236 (s), 753 (s).

2.3.3. Synthesis of 2-(benzothiazole)8-quinolinehydroxylate ([8OQ(oBt)]$^-$)

The $[8OQ(oBt)]^-$was isolated as the sodium salt. First, sodium methoxide was generated by reacting Na metal (4.9 mg, 0.213 mmol) in ~30 mL of methanol (MeOH). Next, a batch of 8OHQ(oBt) (50.7 mg, 0.197 mol) was added and the solution was stirred for ~20 min. The solvent was removed and the orange solid was dried under vacuum.

Quantitative yield. ^{1}H NMR (CD_3OD, 400 MHz, 25 °C, δ from TMS): 8.17 (q, 2H), 8.06 (q, 2H), 7.54 (t, 1H), 7.46 (m, 1H), 7.36 (t, 1H), 6.92 (d, 2H) 6.85 (m, 1H). Selected IR bands: (cm^{-1}) 1575 ($\nu_{N=C}$), 1446 (m), 1095 (m), 717 (s).

*2.3.4. Synthesis of Cu(Q(oBt))$(NO_3)_2(H_2O)\cdot CH_3OH$ (**1**·CH_3OH)*

A batch of Q(oBt) (104 mg, 0.395 mmol) was suspended in MeOH. Separately, $Cu(NO_3)_2\cdot 3H_2O$ (74 mg, 0.395 mmol) was dissolved in ~15 mL of MeOH. The copper solution was then added drop-wise to the ligand suspension resulting in a dark green mixture. The reaction was refluxed for 30 min and stirred for 10 h. After the solution was gravity filtered, slow diffusion of diethylether (Et_2O) resulted in the formation of green crystalline **1** within 24 h. Yield: 156 mg (89%). Selected IR bands: (cm^{-1}) 1595 ($\nu_{N=C}$), 1482 (s), 1268 (s), 761 (s). Electronic absorption spectrum in MeOH: λ_{max} (nm) (ε, M^{-1} cm^{-1}) 211 (47003). Elemental analysis (%): calc. for $C_{17}H_{16}CuN_4O_8S$: C, 40.80; H, 3.2; N, 11.3; S, 6.4. Found: C, 40.7; H, 3.1; N, 11.3; S, 6.2.

*2.3.5. Synthesis of Cu(8OHQ(oBt))$Cl_2\cdot CH_3OH$ (**2**·CH_3OH)*

A batch of 8OHQ(oBt) (240 mg, 0.862 mmol) was suspended in 20 mL MeOH. Separately, $CuCl_2\cdot 2H_2O$ (147 mg, 0.862 mmol) was dissolved in a minimum amount of MeOH, and was added drop-wise to the ligand suspension. The dark orange solution was stirred for 10 h and then gravity filtered. Slow diffusion of Et_2O into the methanolic solution resulted in the formation of dark orange crystalline **2** within 12 h. Yield: 161 mg (84%). Selected IR bands: (cm^{-1}) 3184 (ν_{OH}), 1574 ($\nu_{N=C}$), 1342 (m), 1020 (s), 749 (s). Electronic absorption spectrum in MeOH: λ_{max} (nm) (ε, M^{-1} cm^{-1}) 205 (44316). Elemental analysis (%): calc. for $C_{17}H_{14}Cl_2CuN_2O_2S$: C, 45.9; H, 3.2; N, 6.3; S, 7.2. Found: C, 45.5; H, 2.9; N, 6.3; S, 7.2.

*2.3.6. Synthesis of Cu(8OQ(oBt))Cl(CH_3OH)·CH_3OH (**3**·CH_3OH)*

A batch of $CuCl_2\cdot 2H_2O$ (126 mg, 0.736 mmol) was dissolved in a minimal amount of MeOH and then added drop-wise to freshly prepared Na[8OQ(oBt)] (204 mg 0.736 mmol) in MeOH. The solution immediately turned red and microcrystalline **3** precipitated from the solution. After 10 h, the red brown solid was collected using gravity filtration and dried under vacuum. Yield: 222 mg (70%). Selected IR bands: (cm^{-1}) 1589 ($\nu_{N=C}$), 1455 (s), 1114 (m), 753 (s). Electronic absorption spectrum in MeOH: λ_{max} (nm) (ε, M^{-1} cm^{-1}) 205 (32306). Elemental analysis (%): calc. for $C_{18}H_{17}ClCuN_2O_3S$: C, 49.0; H, 3.9; N, 6.4; S, 7.3. Found: C, 48.8; H, 3.7; N, 6.6; S, 7.7.

*2.3.7. Synthesis of [Cu(8$OH_{1/2}$Q(oBt))(CH_3OH)$(NO_3)]_2(NO_3)$ (**4**)*

First, 8OHQ(oBt) (108 mg, 0.389 mmol) was suspended in 20 mL MeOH. Separately, $Cu(NO_3)_2\cdot 3H_2O$ (73 mg, 0.389 mmol) was dissolved in ~10 mL MeOH. The metal salt was then added drop-wise to the ligand suspension. The deep red solution was stirred for 10 h and gravity filtered. Slow diffusion of Et_2O into the methanolic solution formed orange crystalline **4** within 12 h. Yield: 271 mg (75%). Selected IR bands: (cm^{-1}) 3062 (ν_{OH}), 1567 ($\nu_{N=C}$), 1275 (s), 1010 (m), 749 (s). Electronic absorption spectrum in MeOH: λ_{max} (nm) (ε, M^{-1} cm^{-1}) 203 (46975). Elemental analysis (%): calc. for $C_{34}H_{27}Cu_2N_7O_{13}S_2$: C, 43.7; H, 2.9; N, 10.5; S, 6.9. Found: C, 43.2; H, 2.5; N, 10.5; S, 7.0.

2.4. X-ray data collection and structure solution and refinement

Suitable crystals for X-ray analysis of complexes **1**–**4** were obtained by slow diffusion of Et_2O into separate solutions of each compound dissolved in methanol: complex **1** was isolated as green needles, complex **2** was isolated as orange needles, complex **3** was isolated as red plates and **4** was isolated as orange plates. X-ray diffraction data were collected on a Bruker APEX 2 CCD platform diffractometer (Mo K_α ($\lambda = 0.71073$ Å)) equipped with an Oxford liquid nitrogen cryostream. Crystals were mounted in a nylon loop with Paratone-N cryoprotectant oil. The structures were solved using direct methods and standard difference map techniques, and were refined by full-matrix least-squares procedures on F^2 with SHELXTL (Version 2008) [35]. All non-hydrogen atoms were refined anisotropically. Hydrogen atoms on carbon were included in calculated positions and were refined using a riding model. Crystal data and refinement details are presented in Table 1 for complexes **1**–**4** while selected bond distances and angles are listed in Tables 2 and 3 respectively. The structure of **3**·CH_3OH was found to be non-merohedrally twinned. The two-component orientation matrix produced by CELL_NOW was used to integrate the data which was subsequently scaled and absorption corrected with TWINLABS (V2008/4) [35]. The initial solution was refined with single component data for the stronger domain before final refinement with data from both domains.

2.5. DNA cleavage experiments

Chemical nuclease activity was monitored using agarose gel electrophoresis. SC-DNA was incubated for 30 min at 37 °C in 1.5 mL microcentrifuge tubes containing incubation buffer in a total volume of 15 μL. Complex solutions in 100% dimethylformamide (DMF) were diluted in incubation buffer, resulting in a final DMF concentration of 20% or less. The concentration of complexes was varied from 0 to 50 μM for **1** and **2**, and from 0 to 80 μM for **3**. The concentration of ascorbic acid was twice the concentration of the complex (0–160 μM). When included, DMSO was present at 10% (v/v) and L-histidine was present at 2 mM. After incubation, samples were centrifuged at 12,000 ×*g* in a Mini-Spin microcentrifuge (Eppendorf). A 10 μL sample of the supernatant was removed and mixed with 2 μL of 6× loading dye, then loaded into a well in a 1% (w/v) agarose gel prepared in gel running buffer. The gels were run at 5–8 V/cm for 75 min in gel running buffer, stained in a solution of 0.5 mg/mL EtBr for 30 min, then rinsed in DI water for 10 min before imaging with a UV transilluminator. The relative amounts of DNA after cleavage experiments were determined by dividing the fluorescence intensity of each band by the sum of the fluorescence intensities of all bands in the same lane.

2.6. DNA binding studies

Samples of CT-DNA (12.5 μM) were incubated with ethidium bromide (12.5 μM) and complex **1**, **2** or **3** (0–80 μM) for 30 min at room temperature in a total volume of 10 mL of gel running buffer. Emission spectra were obtained with slit widths of 4 mm, an excitation wavelength of 546 nm and emission wavelengths from 550 to 700 nm. Values for fluorescence intensity were recorded at the λ_{max}. Data were analyzed by Stern–Volmer plots using the equation $I_0/I = K_q[Q] + 1$ [36], where I_0 is the fluorescence intensity of the CT-DNA alone, I is the emission intensity of the CT-DNA plus complex, [Q] is the concentration of the complex, and K_q is the quenching constant. I_0/I vs. [Q] was plotted and the slope of the best-fit line was used to calculate K_q. Binding constants were determined using the equation K_{EtBr} [EtBr] = K_{app} $[complex]_{50\%}$, where K_{EtBr} is the binding constant of EtBr to DNA (1×10^7 M^{-1}) [37], the concentration of ethidium bromide was 12.5 μM, and $[complex]_{50\%}$ is the concentration of complex required to reduce the emission intensity of EtBr by 50% calculated using the Stern–Volmer plot.

2.7. Cell viability assays

For viability assays, cells were plated in 96 well plates at 1000 cells/well and incubated for 24 h before adding copper compounds (concentration range of 0–100 μM) or DMF, the solvent used to dissolve the compounds. Each concentration was assayed in triplicate in each experiment, and all experiments were repeated at least two times. Cell viability was measured 72 h after addition of copper compounds by MTS (3-(4,5-dimethylthiazol-2-yl)-5-(3-carboxymethoxyphenyl)-2-(4-sulfophenyl)-2H-tetrazolium) assay (Promega) according to the manufacturer's instructions and color product measured at 490 nm using an Infinite M200 Pro plate reader controlled by I-control 1.7 software (Tecan,

Table 1
Summary of crystal data and intensity collection and structure refinement parameters for the complexes.

	$Cu(Q(oBt))(NO_3)_2(H_2O)\cdot CH_3OH$ (**1**·CH_3OH)	$Cu(8OHQ(oBt))Cl_2\cdot CH_3OH$ (**2**·CH_3OH)	$Cu(8OQ(oBt))Cl(MeOH)\cdot CH_3OH$ (**3**·CH_3OH)	$[Cu(8OH_{1/2}Q(oBt))(MeOH)(NO_3)]_2(NO_3)$ (**4**)
Empirical formula	$C_{16}H_{12}CuN_4O_7S\cdot CH_3OH$	$C_{16}H_{10}Cl_2CuN_2OS_2\cdot CH_3OH$	$C_{17}H_{13}ClCuN_2O_2S\cdot CH_3OH$	$C_{34}H_{27}Cu_2N_7O_{13}S_2$
Molecular weight	499.94	444.80	440.39	932.83
Crystal color, habit	Green, needle	Orange, needle	Red, plate	Orange, plate
Crystal size (mm)	0.12 × 0.12 × 0.02	0.26 × 0.04 × 0.02	0.25 × 0.11 × 0.02	0.12 × 0.12 × 0.02
Temperature (K)	125(2)	125(2)	125(2)	125(2)
Crystal system	Monoclinic	Monoclinic	Monoclinic	Trilinic
Space group	P2(1)/n	P2(1)/c	P2(1)/c	P-1
Unit cell dimensions				
a (Å)	9.3067(3)	7.7963(1)	6.9815(4)	11.9248(5)
b (Å)	10.9567(4)	12.515(2)	24.4783(1)	12.3516(6)
c (Å)	19.2669(6)	17.827(3)	10.5404(5)	12.8987(6)
α (°)	90	90	90	103.2630(1)
β (°)	96.5430(1)	97.491(2)	92.6260(1)	105.7130(1)
γ (°)	90	90	90	91.4930(1)
V (Å^3), Z	1951.86(1), 4	1724.5(5), 4	1799.41(1), 4	1772.14(1), 2
D_{calc} (mg m^{-3})	1.701	1.713	1.626	1.748
Absorption coeff. (μ, mm^{-1})	1.282	1.711	1.499	1.398
Φ range collected (deg.)	2.13–30.51	1.99–28.45	1.66–30.51	16.9–30.53
Completeness to Φ max (%)	99.9	99.6	100.0	99.1
Reflns collected/unique ($R(int)$)	30885/5963 (0.0379)	223527/4336 (0.0993)	11828/9112 (0.0536)	28931/10749 (0.0263)
Data/restraints/parameters	5963/1/292	4336/0/226	11828/2/244	10749/0/525
R_1, wR_2 ($I>2\sigma(I)$)	0.0507, 0.1281	0.0492, 0.1172	0.0382, 0.0781	0.0389, 0.1011
R_1, wR_2 (all data)	0.0675, 0.1385	0.0818, 0.1318	0.0578, 0.0877	0.0529, 0.1090
Goodness of fit on F^2	1.035	1.044	1.068	1.019
Largest diff peak/hole (e/Å^3)	1.229, −0.802	0.920, −0.811	0.830, −0.430	2.018, −0.892

Research Triangle Park, N.C.). The average background signal from medium without cells was subtracted from all values. The addition of copper compounds did not change the background readings.

To pool data from several experiments, MTS values within each experiment were normalized by setting the average absorbance to 2.0 for wells containing cells and DMF (the vehicle used to dissolve the drug). The normalized value of 2.0 was chosen because it was near the typical absorbance reading per well of cells and DMF. IC50 values were estimated using CalcuSyn Software (Version 2.0; Biosoft, Ferguson, MO, USA).

DNA content per cell was measured by flow cytometry as described previously [38]. Briefly, cells were removed from tissue culture plastic by incubation in trypsin, pelleted and re-suspended in 0.5 mL phosphate buffered saline (PBS) at a concentration of ~1 × 10^7 cells/mL. Seventy percent ice cold ethanol was added to fix the cells. Cells were rehydrated by pelleting and re-suspension in PBS; they were then pelleted again and re-suspended in a DNA staining solution (PBS supplemented with 2 mg/100 μL propidium iodide, 0.2 mg/mL RNAse A, 0.1% NP-40). A Becton Dickinson FACSCanto II, controlled by BD FACSDiva software (Mountain View, CA) was used to measure propidium iodide (DNA content) per cell.

Table 2
Selected bond distances (Å) for metal complexes.

$Cu(Q(oBt))(NO_3)_2(H_2O)\cdot CH_3OH$ (**1**·CH_3OH)			
Cu–N(1)	2.252(2)	Cu–O(1)	1.934(2)
Cu–N(2)	2.025(2)	Cu–O(2)	1.998(2)
Cu–O(5)	2.005(2)		
$Cu(8OHQ(oBt))Cl_2\cdot CH_3OH$ (**2**·CH_3OH)			
Cu–N(1)	1.966(3)	Cu–O(1)	2.207(3)
Cu–N(2)	2.066(3)	Cu–Cl(2)	2.4375(1)
Cu–Cl(1)	2.1946(1)		
$Cu(8OQ(oBt))Cl(MeOH)\cdot CH_3OH$ (**3**·CH_3OH)			
Cu–N(1)	1.937(2)	Cu–O(1)	2.0164(2)
Cu–N(2)	2.149(2)	Cu–O(2)	2.236(2)
Cu–Cl	2.2091(7)		
$[Cu(8OH_{1/2}Q(oBt))(MeOH)(NO_3)]_2(NO_3)$ (**4**)			
Cu(1)–N(11)	1.9228(2)	Cu(1)–O(11)	2.0825(2)
Cu(1)–N(12)	2.0936(2)	Cu(1)–O(12)	2.1967(2)
Cu(1)–O(13)	1.9357(2)	Cu(2)–O(21)	2.1151(2)
Cu(2)–N(21)	1.9228(2)	Cu(2)–O(22)	2.2024(2)
Cu(2)–N(22)	2.0922(2)	Cu(2)–O(23)	1.9207(2)

Table 3
Selected bond angles (°) for metal complexes.

$Cu(Q(oBt))(NO_3)_2(H_2O)\cdot CH_3OH$ (**1**·CH_3OH)			
N(1)–Cu–N(2)	78.26(9)	N(2)–Cu–O(1)	167.06(1)
N(1)–Cu–O(1)	114.63(1)	N(2)–Cu–O(2)	91.25(9)
N(1)–Cu–O(2)	87.73(8)	N(2)–Cu–O(5)	95.28(1)
N(1)–Cu–O(5)	84.30(9)	O(1)–Cu–O(2)	88.24(1)
O(1)–Cu–O(5)	87.51(1)	O(2)–Cu–O(5)	168.46(1)
$Cu(8OHQ(oBt))Cl_2\cdot CH_3OH$ (**2**·CH_3OH)			
N(1)–Cu–N(2)	79.22(1)	N(2)–Cu–O(1)	153.94(1)
N(1)–Cu–O(1)	76.08(1)	N(2)–Cu–Cl(1)	103.19(9)
N(1)–Cu–Cl(1)	154.86(1)	N(2)–Cu–Cl(2)	101.31(9)
N(1)–Cu–Cl(2)	98.86(9)	O(1)–Cu–Cl(1)	95.79(7)
O(1)–Cu–Cl(2)	90.63(8)	Cl(1)–Cu–Cl(2)	105.06(4)
$Cu(8OQ(oBt))Cl(MeOH)\cdot CH_3OH$ (**3**·CH_3OH)			
N(1)–Cu–N(2)	72.29(8)	N(2)–Cu–O(1)	157.79(8)
N(1)–Cu–O(1)	81.27(8)	N(2)–Cu–O(2)	90.14(8)
N(1)–Cu–O(2)	97.36(8)	N(2)–Cu–Cl	101.33(6)
N(1)–Cu–Cl	162.90(6)	O(1)–Cu–O(2)	98.33(8)
O(1)–Cu–Cl	97.45(6)	O(2)–Cu–Cl	99.69(5)
$[Cu(8OH_{1/2}Q(oBt))(MeOH)(NO_3)]_2(NO_3)$ (**4**)			
N(11)–Cu(1)–N(12)	79.24(7)	N(12)–Cu(1)–O(11)	157.97(7)
N(11)–Cu(1)–O(11)	79.49(7)	N(12)–Cu(1)–O(12)	97.40(7)
N(11)–Cu(1)–O(13)	174.57(7)	N(12)–Cu(1)–O(13)	101.46(7)
O(11)–Cu(1)–O(13)	99.18(7)	O(11)–Cu(1)–O(13)	87.85(7)
N(21)–Cu(2)–N(22)	79.20(7)	N(22)–Cu(2)–O(21)	157.61(7)
N(21)–Cu(2)–O(21)	79.11(7)	N(22)–Cu(2)–O(22)	99.21(7)
N(21)–Cu(2)–O(23)	172.85(8)	N(22)–Cu(2)–O(23)	102.452(7)
O(21)–Cu(2)–O(23)	98.36(7)	O(22)–Cu(2)–O(23)	88.09(8)

3. Results and discussion

3.1. Syntheses and characterization of ligands and complexes

The ligands were prepared via a condensation reaction between the quinoline containing aldehyde and ABT in anhydrous methanol. These types of reactions usually result in the formation a Schiff base except when ABT is used as the amine.

In these cases, the imine cyclizes to form a benzothiazoline (Bt) group [39–42] (Scheme 1) which can then undergo oxidation to form the corresponding benzothiazole (oBt) (Scheme 2). A variety of oxidative techniques employing several different oxidants have been utilized in the Bt → oBt conversion [43–45], however we have found that most readily oxidize in solution in the presence of air yielding a quantitative amount of benzothiazole [46,47].

The Bt → oBt transformation can be monitored using ^{1}H NMR spectroscopy; in particular the –NH of the benzothiazoline group resonates between ~4.4 and 5.1 ppm and the thiazoline CH is found as a singlet between ~6.1 and 6.7 ppm. Upon oxidation both of these resonances disappear and there is a concomitant downfield shift of the ring resonances to above 7 ppm, presumably due to the extended conjugation between the two ring systems upon oxidation [46]. Interestingly, during the synthesis of Q(oBt) no benzothiazoline was noted while a mixture of 8OHQ(Bt) and 8OHQ(oBt) was obtained in the analogous synthesis. These findings further confirm that the substituent at the 2-position in the substituted benzothiazoline plays a fundamental role in governing the susceptibility toward oxidation in these types of molecules [46,47].

Complexes **1**–**4** were obtained by reaction of the ligands with either $Cu(NO_3)_2\cdot XH_2O$ (**1**, **2** and **4**) or $CuCl_2\cdot 2H_2O$ (**3**) in MeOH. The compounds were obtained in good yield and characterized by elemental analysis, UV/Vis, IR and single crystal X-ray diffraction. The initial ligation reactions with Q(oBt) were carried out with $CuCl_2\cdot 2H_2O$ however these attempts resulted in brown heterogeneous reaction mixtures from which no crystalline product could be obtained. Similar reactions utilizing $Cu(NO_3)_2\cdot XH_2O$ as the starting metal salt resulted in a dark olive green, homogeneous solution from which green crystalline **1**, $Cu(Q(oBt))(NO_3)_2(H_2O)$, was obtained. Complex **2**, $Cu(8OHQ(oBt))(MeOH)(NO_3)$, was obtained in a similar reaction by suspending 8OHQ(oBt) in MeOH and adding a methanolic solution of $CuCl_2\cdot 2H_2O$. The reaction immediately became homogeneous and changed color to bright red and yielded red crystalline **2** upon slow diffusion of Et_2O. Interestingly, analogous reactions with 8OHQ(oBt) and $Cu(NO_3)_2\cdot XH_2O$ as the starting salt yielded complex **4**. The X-ray crystal structure of **2** revealed an unexpected coordinated –OH group while the structure of **4** showed there were two Cu(8OHQ(oBt)) groups in the unit cell however one copper center contained a deprotonated hydroxyl group while on the other copper center the hydroxyl group remained protonated. These findings prompted us to isolate the deprotonated analog, **3**. Similar reactions were carried out with $Cu(NO_3)_2\cdot XH_2O$ and $CuCl_2\cdot 2H_2O$ with freshly prepared Na[8OQ(oBt)], however all reactions with the nitrate salt were unsuccessful. The IR spectra for complexes **1**–**4** have medium intensity bands ~1580 cm^{-1} which is assigned the thiazole $\nu_{N=C}$ [46,48]. Complexes **2** and **4** also exhibit a ν_{OH} resonance at 3064 and 3062 cm^{-1}, respectively.

3.2. X-ray crystallographic studies

3.2.1. Structure of $Cu(Q(oBt))(NO_3)_2(H_2O)\cdot CH_3OH$ (**1**·CH_3OH)

The structure of complex **1** is shown in Fig. 1. The neutral, five coordinate Cu(II) center contains an N_2O_3 coordination sphere that is composed of one bidentate Q(oBt) ligand (N,N coordinated), two nitrate ions from the starting material and a water molecule. There is also one MeOH of crystallization present in the crystal lattice. Determination of the geometry of the compound was done by analysis of the trigonality index, $\tau = (\alpha-\beta)/60$, where α and β are the two largest bond angles around the Cu(II) and τ values of 0 and 1 are assigned to perfect square pyramidal (SP) and trigonal bipyramidal (TBP) geometries, respectively. For complex **1**, $\tau = 0.023$ and, as such, the geometry is best described as slightly distorted square pyramidal [49–51]. The Jahn–Teller effect is very common among Cu(II), d^9, octahedral complexes however for five coordinate species secondary Jahn–Teller effects dominate. The secondary Jahn–Teller effect can be observed for both SP and TBP geometries and is due to the non-degenerative electronic ground state mixing with a low lying degenerative excited state which ultimately causes an overall lowering of the ground state energy [52]. However, in order to properly attribute structural differences in five coordinate complexes to secondary Jahn–Teller effects, it has been deemed necessary to have a series of well-defined complexes with similar coordination spheres [53]. As such, the discussion of structural variation within and between the complexes reported here will not be extrapolated to secondary Jahn–Teller effects.

The $Cu-N_{quinoline}$ ($Cu-N_Q$) and $Cu-N_{thiazole}$ bond lengths in complex **1** are 2.252(2) and 2.025(2) Å respectively, with the longer $Cu-N_Q$ occupying the axial site. All bond lengths in the basal plane are more than 0.200(2) Å shorter than the axial $Cu-N_Q$ length. The Cu-nitrate bond lengths are nearly equivalent with Cu–O(2) and Cu–O(5) distances of 1.998(2) and 2.005(2) Å, respectively. The Cu–water bond distance is slightly shorter at 1.934(2) Å. All distances are within the range of those observed for similar compounds [46,54,55]. There are two hydrogen bonding interactions within the crystal lattice between adjacent molecules as well as with the interstitial MeOH (Fig. 2). The MeOH participates as both a hydrogen bond acceptor and donor: 1) H1S of the solvent to the ligated NO_3^- (O5) and 2) O1S of the solvent to H1B of the water bound to CuA. There is also a direct hydrogen bond interaction between the complexes from the bound nitrate (O3A) to the water (H1A).

3.2.2. Structure of $Cu(8OHQ(oBt))Cl_2\cdot CH_3OH$ (**2**·CH_3OH)

The structure of **2** is shown in Fig. 3. The Cu complex is comprised of one tridentate 8OHQ(oBt) ligand coordinated in an N,N,O–H fashion and two chloride ions. Here, the trigonality index is $\tau = 0.015$ indicating this complex also approximates a square pyramidal geometry with slightly less deviation than observed in **1**. Similar lengthening of the axial bond length is observed in complex **2**, with this bond measuring more than 0.200(1) Å longer than the bond lengths found in the plane. Unlike complex **1**, where N_Q occupies the axial site, complex **2** has Cl(2) in this position with a CuCl(2) distance of 2.4375(1) Å, while the Cu–Cl(1) measures 2.1946(1) Å. The change in the axial ligand is likely due to the tridentate nature of the 8OHQ(oBt) ligand frame. The $Cu-N_Q$ and $Cu-N_{thiazole}$ bond lengths are 2.066(3) and 1.966(3) Å, respectively, while the Cu–O(1) bond length measures 2.207(3) Å. There are a handful of copper complexes that contain ligated protonated –OH group [56,57]

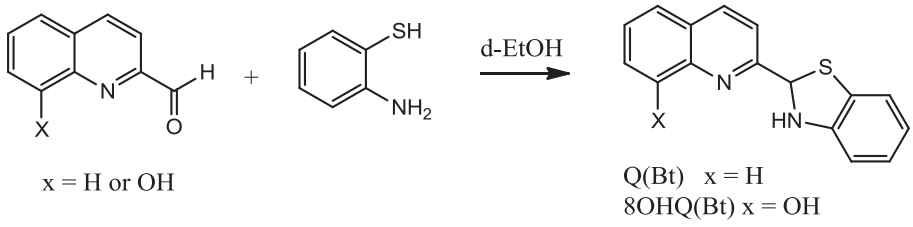

Scheme 1. Formation of the quinoline benzothiazoline (Bt) from ABT and the aldehyde.

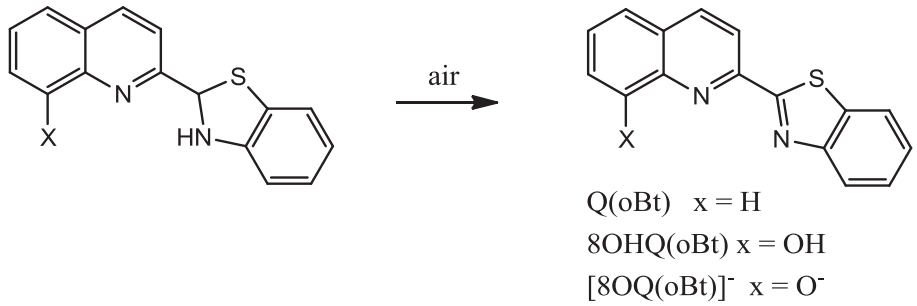

Scheme 2. Bt → oBt conversion showing the oxidation of the benzothiazoline group to the benzothiazole.

and the Cu – O(1) bond lengths presented here are within the range of those previously reported. The hydroxyl proton H(1) participates in a hydrogen bonding interaction with the methanol solvent of recrystallization. All bond distances are in the range of previously reported copper complexes with N and O type donor atoms [46,58].

3.2.3. Structure of Cu(8OQ(oBt))Cl(CH_3OH)·CH_3OH (**3**·CH_3OH)

The structure of complex **3** is shown in Fig. 4. Similar to complex **2**, the ligand frame binds in a tridentate N,N,O fashion. The coordination sphere is completed by one chloride ion and one methanol. This five coordinate, neutral species has $\tau = 0.085$ indicating, like complexes **1** and **2**, the geometry of complex **3** can be assigned as distorted square pyramid. Within the crystal lattice, a solvent methanol molecule participates in H-bonding between the deprotonated hydroxyl group of the ligand frame and the coordinate methanol. This interaction forms a 1-D hydrogen bonding chain that runs down the crystallographic a-axis. The axial Cu – O(2) methanol bond distance measures 2.236(2) Å, a distance that is only slightly longer than the bond lengths within the basal plane. The Cu – N_Q and Cu – $N_{thiazole}$ bond lengths are 1.937(2) and 2.149(2) Å, respectively, while the Cu – O(1) (hydroxylate) measures 2.0164(2) Å and the Cu – O(2) (bound methanol) bond distances is 2.236(2) Å. The ~0.200(2) Å difference in the Cu – O bond lengths can be attributed to the negative charge of O(1) resulting in a stronger interaction with the copper. The Cu – Cl bond length in **3** is 2.2091(7) Å, a distance that is comparable to the equatorial Cu – Cl(1) in complex **2**.

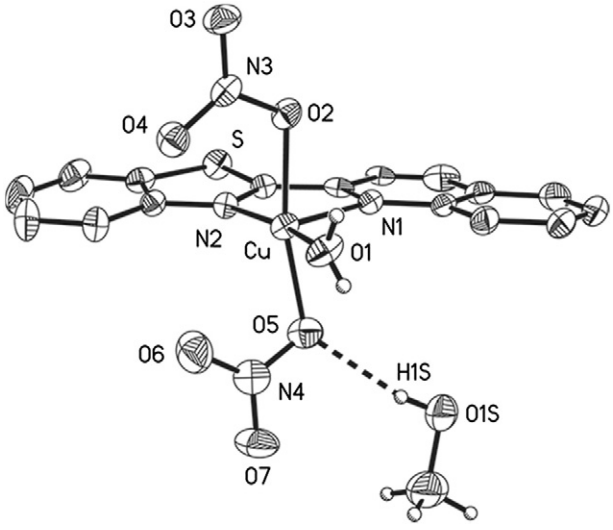

Fig. 1. Thermal ellipsoid plot (50% probability level) of complex **1**·MeOH showing the numbering scheme. The aromatic hydrogen atoms have been omitted for clarity.

3.2.4. Structure of [Cu(8$OH_{1/2}$Q(oBt))(CH_3OH)(NO_3)]$_2$(NO_3) (**4**)

In this complex, the ligand frame binds in an N,N,O tridentate fashion, similar to the structure of **2** and **3**, however the structure revealed that there is only *one* hydroxyl proton for every two ligand frames. The complexes are oriented within the lattice such that one –OH hydrogen is shared between two ligand frames. This results in an overall 'half-protonation' of the ligand giving rise to an overall +1 charge and one nitrate counter ion for every two complexes. The N_2O_3 coordination sphere around each metal center is completed by a ligated NO_3^- ion and one methanol. The structure of **4**, showing the shared hydrogen atom as well as hydrogen bonding interactions between the counter ion and the bound solvent, is shown in Fig. 5. Both five coordinate complexes within the unit cell adopt a distorted square pyramidal geometry with $\tau = 0.276$ for Cu(1) and 0.254 for Cu(2) and contain nearly identical coordination spheres. The Cu – N_Q bond is *trans* to ligated NO_3^- and measures 1.9228(2) Å (Cu(1) – N(12) and Cu(2) – N(22)) in both complexes. Likewise, all of the analogous Cu – O bond distances between the two complexes are very similar: the Cu – O_{NO3} bond lengths (Cu(1) – O(13) and Cu(2) – O(23)) differ by 0.015(2) Å, the Cu – O_{MeOH} (Cu(1) – O(12) and Cu(2) – O(22)) differ only by ~0.006(2) Å and the Cu – $O_{hydroxyl}$ distances (Cu(1) – O(11) and Cu(2) – O(21)) differ by 0.0326(2) Å. The most noticeable difference in bond lengths between the two copper centers involves the Cu – $N_{thiazole}$ distance that measures 2.1967(2) and 2.0922(2) Å for Cu(1) – N(12) and Cu(2) – N(22), respectively, a $\Delta \approx 0.1045(2)$ Å. In both complexes the Cu – $N_{thiazole}$ bond is ligated trans to the Cu – $O_{hydroxyl}$ and thus utilize the same orbital set for bonding. It is possible that O(11) adopts more hydroxylate character, exerting a greater *trans* influence thus lengthening the Cu(1) – $N_{thiazole}$ bond, a trend that is also seen in complexes **2** and **3**. Conversely, there seems to be little correlation between the Cu – $O_{hydroxyl}$ bond lengths observed in **4**; the protonated Cu – $O_{hydroxyl}$ bond distance in **2** measures 2.207(3) Å while the Cu – $O_{hydroxlate}$ in **3** is 2.0164(2) Å, a $\Delta \approx 0.190(2)$ Å while the analogous Cu – O bond distances in **4** are 2.0825(2) and 2.1151(2) Å. The axial ligated MeOH has an average Cu – O_{MeOH} bond length of 2.1996(2) Å, a distance that is comparable to bond lengths within the plane.

3.3. EtBr displacement assay

DNA is the pharmacological target of several metallo-chemotherapeutics and therefore the interaction between DNA and complexes **1**–**3** is of interest [2,59]. The ability of complex **1**–**3** to interact with DNA was assessed by competitive ethidium bromide (EtBr) displacement studies. This assay relies on intense fluorescence near ~600 nm due to EtBr intercalated between adjacent base pairs. In the presence of a competitive intercalator, the EtBr can be displaced with a subsequent decrease in fluorescence intensity that is attributed to solvent quenching [60,61]. For complexes **2** and **3**, the emission intensity ($\lambda_{ex} = 546$ nm) for the EtBr-DNA adduct decreases with an increase in complex concentration. This relationship is shown in Fig. 6 for compound

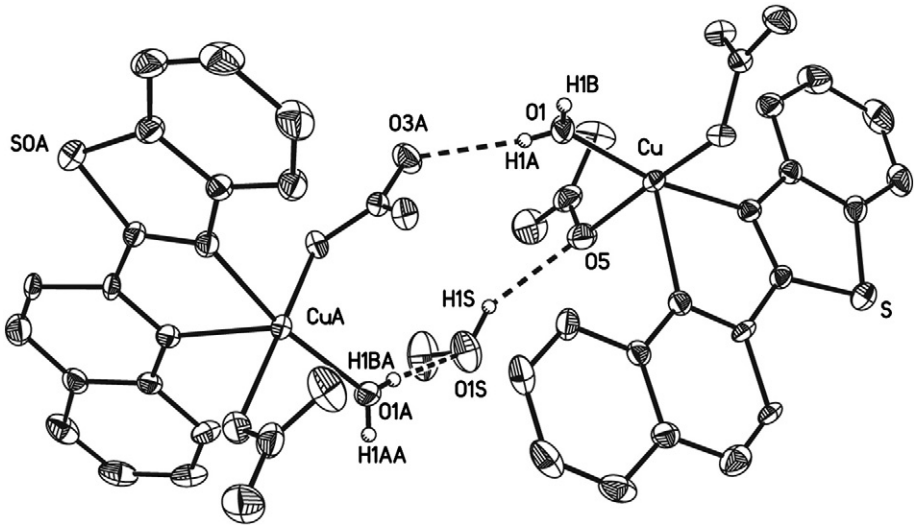

Fig. 2. Thermal ellipsoid plot (50% probability level) of **1**·MeOH showing the hydrogen bonding between two compounds as well as the associated numbering scheme. The aromatic hydrogen atoms have been omitted for clarity.

2 and Fig. 7 for compound **3**. The observed decrease in emission intensity suggests that both **2** and **3** competitively intercalate DNA and effectively compete with EtBr to bind the hydrophobic regions of the DNA duplex. The displacement studies with complex **1** were inconclusive due to the formation of a precipitate during these reactions. The apparent binding constants (K_{app}) for **2** and **3** were derived by plotting the fluorescence intensity versus complex concentration following the classical Stern–Volmer equation, then using the relationship $K_{EtBr}[EtBr] = K_{app}[complex]_{50\%}$, where $K_{EtBr} = 1 \times 10^7\ M^{-1}$ (Inset, Fig. 6 (**2**) and 7 (**3**)) [36,37]. The magnitude of the binding constants are **2** $= 1.47 \times 10^7\ M^{-1}$ and **3** $= 3.09 \times 10^7\ M^{-1}$ (Fig. 7, inset). The similar planar ligand frames and extended aromatic conjugation present in both complexes is reflected in the comparable binding constants. These K_{app} values are several orders of magnitude larger than other previously reported Cu(II) complexes [15,21,26,27] but are in the range of known classical intercalators and metallointercalators [62].

3.4. Nuclease activity

Artificial nucleases typically produce a sequential transition between super-coiled (I), single-nicked (II) and double-nicked (III) DNA. Each scission changes the overall structure of the DNA fragment and is thus identifiable via gel electrophoresis. Super coiled DNA (I) is the native, uncut plasmid DNA that is obtained from *Escherichia coli*, appears as the band of lowest mass and travels the furthest on the gel; single-nicked (II) represents a form of relaxed DNA in which only one strand is cleaved, its relaxed form causes it to appear as the band of highest mass and travel the shortest distance on the gel; and double-nicked (III), represents a linearized plasmid with both strands cleaved and appears between the super coiled and single nicked bands.

The cleavage activities of complexes **1**–**3** were studied in the presence of 2 equivalents of ascorbic acid. Control experiments were also performed with ascorbic acid and free ligand in the absence of complex and no DNA cleavage was noted. Concentration dependent cleavage was observed for all complexes and each convert supercoiled DNA (I) to single-nicked (II) with concentrations of less than 10 μM complex. The gel electrophoresis results for complexes **1**–**3** are shown in Fig. 8. The low concentration required to observe cleavage activity indicates that these complexes exhibit effective and efficient nuclease activity compared to other previously reported copper compounds [16,37,63–65]. Complexes **1**–**3** continue to promote cleavage to produce double nicked DNA (III) at concentrations as low as 20 μM complex. The overall reactivity differences within this set of compounds is ordered **2** > **1** > **3**, with **2** more rapidly and efficiently cleaving DNA. A comparison of reactivity between complexes **1**–**3** at two separate concentrations, 20 and 50 μM, is shown in Fig. 9. At 20 μM concentration of complex **2**, no super-coiled DNA (I) remains while at the same concentrations of complexes **1** and **3**, 8% and 21%, respectively, of form (I) is left. Complexes **1** and **3** also initiate double strand cleavage at concentrations greater than 20 μM (Fig. 9). Interestingly, for complex **2** concentrations > 50 μM, fragmented DNA is observed due to the occurrence of multiple strand scissions. The observed intense activity of these complexes, combined with the relatively short incubation time (30 min at 37 °C, pH = 7.2), substantiates the classification of these species as highly potent nucleases.

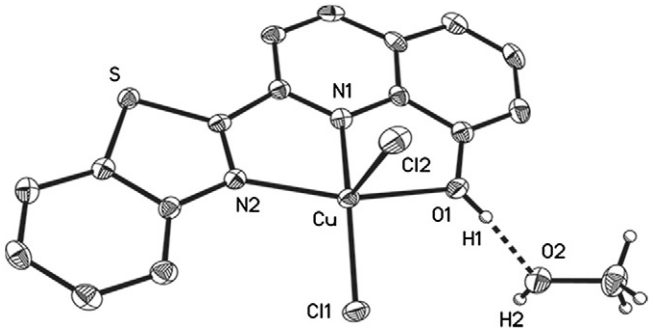

Fig. 3. Thermal ellipsoid plot (50% probability level) of complex **2**·MeOH showing the numbering scheme. The aromatic hydrogen atoms have been omitted for clarity.

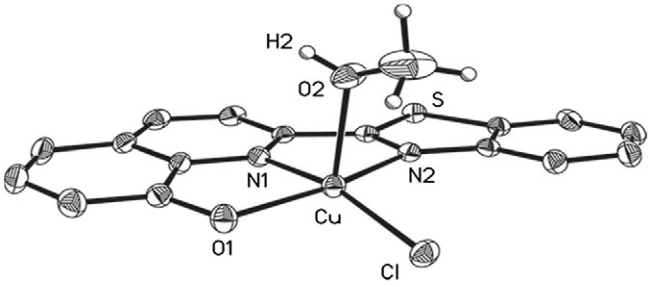

Fig. 4. Thermal ellipsoid plot (50% probability level) of complex **3** showing the numbering scheme. The aromatic hydrogen atoms have been omitted for clarity.

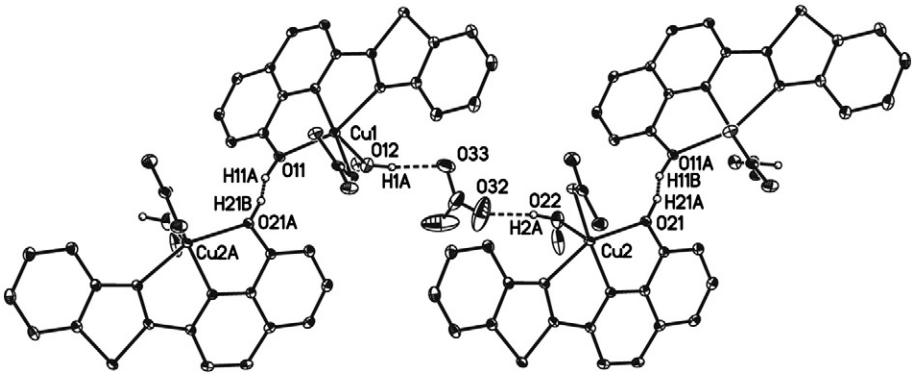

Fig. 5. Thermal ellipsoid plot (50% probability level) of complex **4** showing the numbering scheme. The shared hydrogen between the 8OHQ(oBt) and 8OQ(oBt)− are depicted as two different hydrogen atoms to show the hydrogen bonding network. Aromatic hydrogen atoms have been omitted for clarity.

A comparative analysis of the structural variations in complexes **1**–**3**, particularly in the quinoline portion of the ligand frame, may provide additional insight into the observed nuclease differences. The presence of the phenyl group at the 8th carbon seems to play a noteworthy role in dictating the reactivity. It may be that the protonated hydroxyl group in **2** enhances the hydrogen bonding capacity between the complex and DNA thus positively influencing cleavage efficacy. Conversely, the negative phenylato oxygen donor in **3** may have less favorable electrostatic interactions with the negatively charged backbone of DNA.

3.4.1. Nuclease activity in the presence of radical scavengers

There are two possible mechanisms known to play a role in the cleavage by metallonucleases: hydrolytic and oxidative. The hydrolytic mechanism of cleavage relies on the inductive effects of the copper on the phosphate backbone. This interaction increases the susceptibility of the phosphate backbone toward nucleophilic attack by bulk water or hydroxide thus producing the linearization of DNA observed as a result of complex cleavage [16]. The oxidative mechanism of cleavage functions primarily through the production of reactive oxygen species (ROS) and can include hydroxyl radical (•OH) and singlet oxygen ($^1O_2$) species that are produced via the Cu(II)/Cu(I) redox couple [66].

Differentiation between hydrolytic and oxidative mechanisms can be accomplished using ROS scavengers such as dimethyl sulfoxide and L-histidine, which scavenge for •OH and $^1O_2$, respectively. Cleavage ability by complexes that utilize a hydrolytic pathway will not be affected by the addition of the ROS scavengers, however complexes utilizing an oxidative mechanism will exhibit dampened nuclease ability. To elucidate the mechanism of DNA strand scission by complexes **1**–**3** (hydrolytic or oxidative), cleavage reactions were carried out in the presence of DMSO or L-histidine. The results of these studies are presented in Fig. 10.

The DMSO studies with complex **1** revealed no change in nuclease activity. Similar studies with **2** and **3** however, revealed that neither complex can completely convert super-coiled DNA (I) to single-nicked (II) with concentrations of up to 50 μM complex. Additionally, complex **2** produced no double-nicked DNA (form III) in the presence of DMSO while complex **3** was only able to produce minimal amounts of form (III) at 30–40 μM. In the absence of DMSO, complete conversion of form (I) → (II) was observed at 30 μM for both complexes **1** and **2**. The lower nuclease efficacy of complexes **2** and **3** in the presence of DMSO indicates that both of these complexes utilize an oxidative pathway during DNA cleavage with •OH playing an important role, especially in the conversion of form (II) to (III). Conversely, the OH radical is not apparent in cleavage reactions with complex **1**. Concentration dependent cleavage reactions with complexes **1**–**3** in the presence of L-histidine showed a constant amount of super-coiled DNA (I) with no appreciable increase in forms (II) or (III) up to 50 μM of each complex. Overall, these results suggest that complexes **1**–**3** utilize an oxidative mechanism to cleave DNA. There have been previous reports of DNA cleavage by copper complexes utilizing one [16,35] or multiple ROS [37]. Here it appears that $^1O_2$ species play a primary role in the cleavage by complexes **1**–**3** with •OH radicals performing a more secondary role in the reactivity of complexes **2** and **3**.

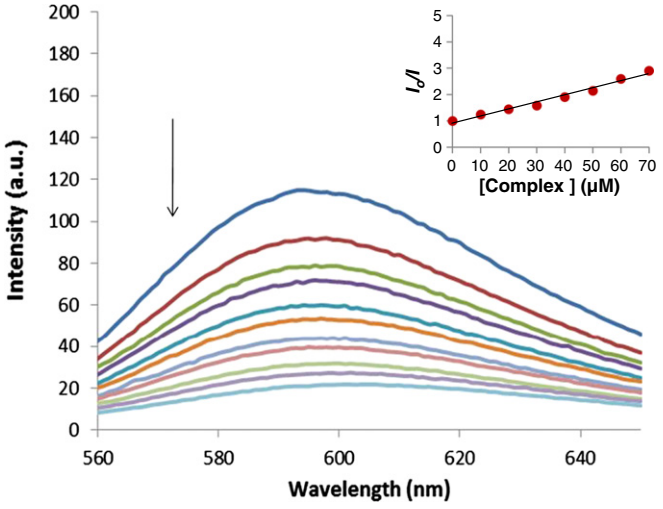

Fig. 6. Fluorescence quenching of EtBr-DNA by complex **2** with concentrations of 0 to 100 μM of complex. The arrow indicates the fluorescence decreases as the concentration of the complex increases. Inset: Plot of I/I_o versus [2], $\lambda_{em} = 595$ nm.

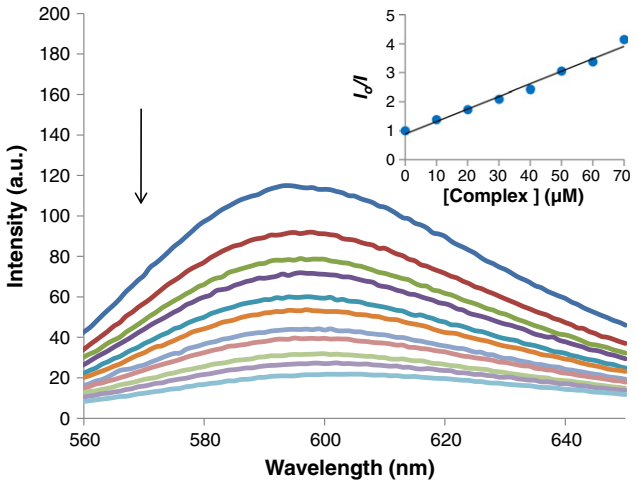

Fig. 7. Fluorescence quenching of EtBr-DNA by complex **3** with concentrations of 0 to 100 μM of complex. The arrow indicates the fluorescence decreases as the concentration of the complex increases. Inset: Plot of I/I_o versus [**3**], $\lambda_{em} = 595$ nm.

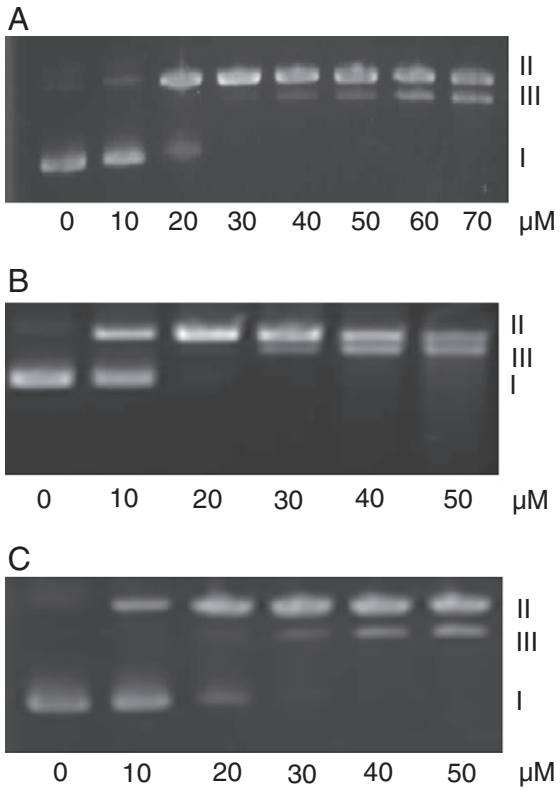

Fig. 8. DNA cleavage by complexes **1** (A), **2** (B) and **3** (C) from 0 to 50 μM of complex in the presence of 2 equivalents ascorbic acid.

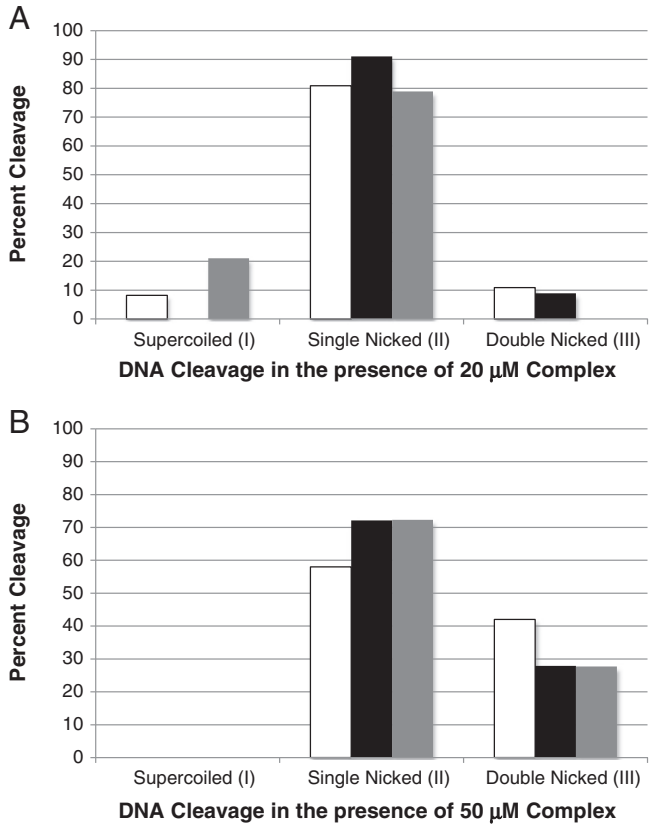

Fig. 9. Cleavage of SC-DNA by complexes **1** (white), **2** (black), and **3** (gray) in the presence of 2 equivalents of ascorbic acid. At lower concentrations of complex (A, 20 μM) most of the DNA is in the single nicked form (II). At higher concentrations (B, 50 μM), a significant fraction has been converted to the double nicked form (III).

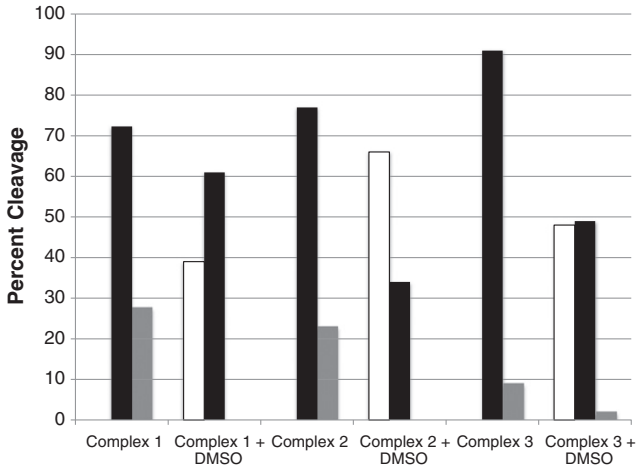

Fig. 10. ROS scavenger studies: Cleavage of SC-DNA by 30 μM complexes **1**–**3** in the absence and presence of 10% DMSO. SC-DNA (Form I, white) is converted to nicked DNA (Form II, black) and then to double nicked DNA (Form III, gray) at a decreased rate in the presence of DMSO. With L-histidine, addition of complexes did not cause any DNA nicking above buffer controls.

3.5. Cytotoxicity evaluation

The anticancer activity of complexes **1**–**3** against HeLa cells was investigated. The cells were challenged with each of **1**–**3**, over a range of concentrations up to 100 μM, for 72 h and cell viability measured by MTS assay. Each of the complexes tested decreased cell viability, as shown in Fig. 11, all with IC50 values in the micromolar range. Compound **3** exhibited the greatest inhibitory effect with an IC50 value of 6.5 μM. The IC50 values for **1** and **2** are 53 μM and 21 μM, respectively. The overall inhibitory effect on cell viability of the complexes is ordered **3** > **2** > **1**.

Copper compounds are known to induce DNA damage, which can slow cell cycle progression [15–17]. To examine whether compounds **1**–**3** blocked cells at a specific cell cycle stage, DNA content per cell was measured by flow cytometry at 24 and 48 h after compound addition. As shown in Fig. 12, for cells incubated for 48 h in 25 μM of each compound, the distribution of cell cycle stages was unchanged by these copper compounds. Additionally, a population of cells with less than G1 DNA content was also present which is consistent with apoptotic cells. It is possible that copper-induced DNA damage is not confined to a specific cell cycle stage, but instead is occurring throughout the cell cycle.

4. Conclusion

Complexes **1**–**3** exhibit potent concentration dependent nuclease activity and promote both single and double strand cleavage of DNA at concentrations as low as 20 μM in 30 min. Despite the similarities in the coordination spheres of the complexes, we see a distinct difference in the overall nuclease ability within the set with **2** > **1** > **3**. This suggests the presence of the OH group and the charge on the phenyl ring is important in modulating the observed reactivity which may be related to the electrostatic interaction between the complex and duplex DNA. Mechanistic studies utilizing DMSO and L-histidine indicate that all complexes utilize an oxidative mechanism with both $^1O_2$ and •OH required for optimal activity. Studies on human HeLa cells indicate complexes **1**–**3** have high in vitro cytotoxic properties with IC50 values in the range of 6–53 μM with **3** > **2** > **1**. Given that the distribution of cell cycle stages remains unchanged when complexes are present, DNA damage may be occurring throughout the cell cycle. Furthermore, it is likely that other non-oxidative mechanisms (proteasome inhibition or non-apoptotic pathways) are contributing to cell death due to the

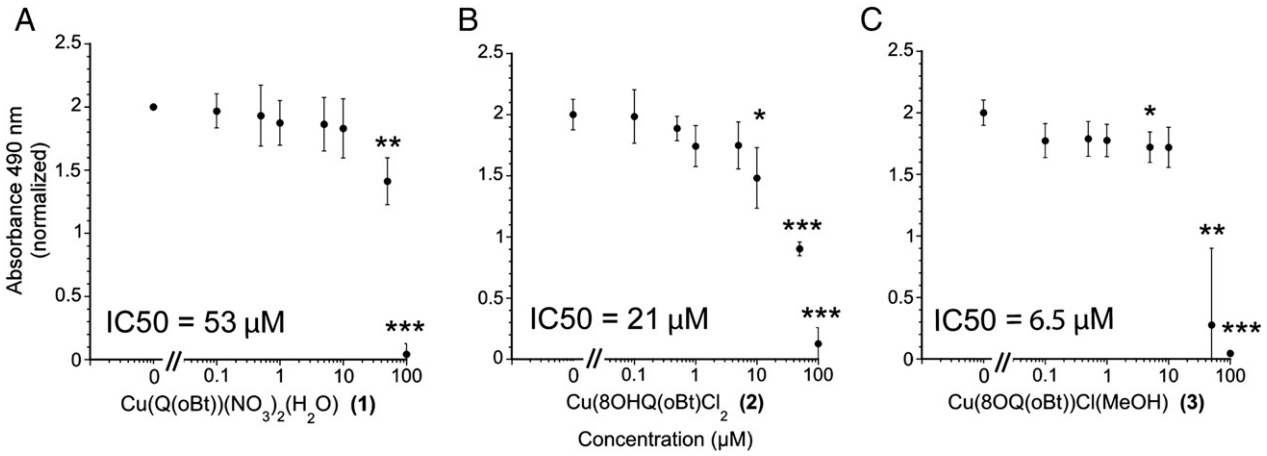

Fig. 11. Effect of complexes **1**–**3** on the cell viability of HeLa cells. The cells were incubated with the compounds with increasing concentration from 0.1 μM–100 μM. Viability was measured after 72 h incubations by MTS assays. Data are shown as mean ± SD. Values statistically different from vehicle-control treated cells are shown by: *$p < 0.05$; **$p < 0.01$; ***$p < 0.001$. Plots show data pooled from 3 independent experiments.

greater cytotoxicity of **3** compared to **2**. Investigations into the cell death mechanism as well as studies that delineate the contributions of the thiazole versus the quinoline moiety in the observed reactivity are aims of our further research.

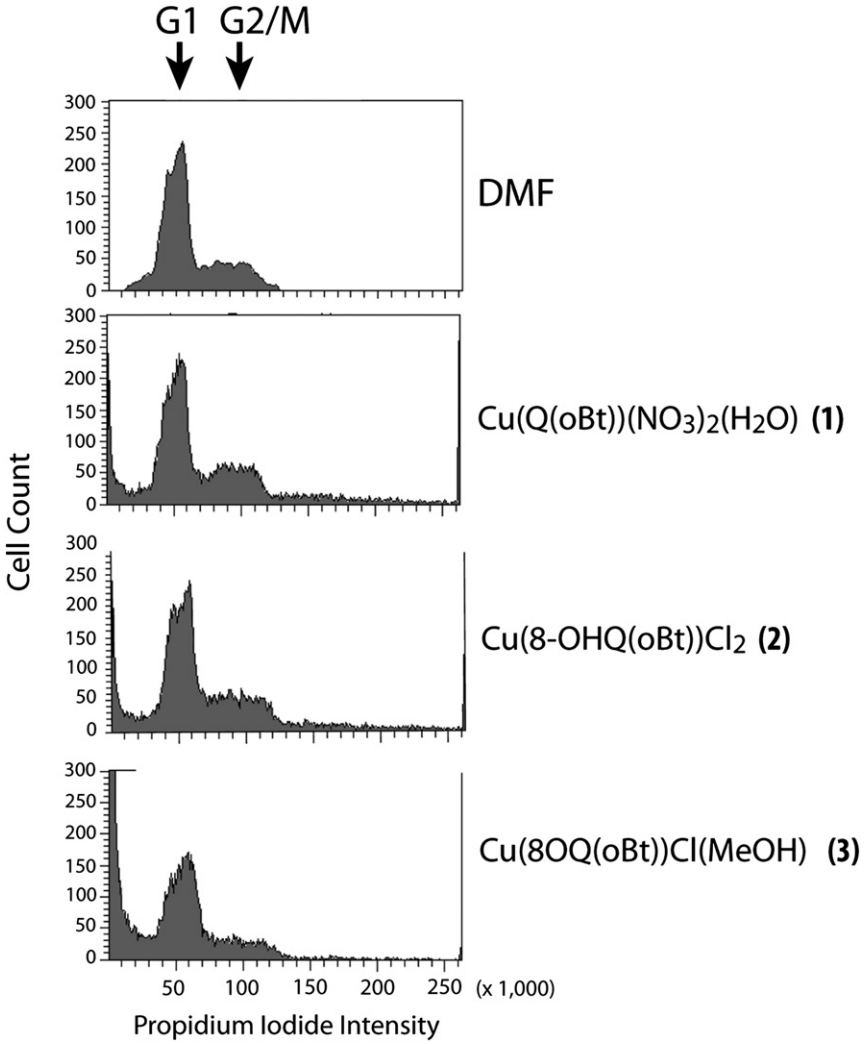

Fig. 12. Effects of complexes **1**–**3** on the cell cycle of HeLa cells. The cells were treated with DMF or compounds **1**–**3** at 25 μM for 48 h. DNA content per cell was measured by propidium iodide staining and positions of G1 and G2/M cell cycle stages noted above the plots. The data are representative of three separate experiments.

Acknowledgments

Union College is thanked for its generous financial support, startup grant and the Faculty Research Fund (LAT, KMF). We also thank the National Science Foundation (NSF 0521237) for supporting the X-ray diffraction facility at Vassar College (JMT).

Appendix A. Supplementary material

CCDC 978338, 978336, 979281, and 979188 contain the supplementary crystallographic data for Cu(Q(oBt))$(NO_3)_2(H_2O)\cdot CH_3OH$ (**1** · CH_3OH), Cu(8OHQ(oBt))Cl_2 · CH_3OH (**2** · CH_3OH), Cu(8OQ(oBt))Cl(CH_3OH) ·CH_3OH (**3** · CH_3OH) and [Cu($8OH_{1/2}$Q(oBt))(MeOH)$(NO_3)]_2(NO_3)$ (**4**), respectively. These data can be obtained free of charge from The Cambridge Crystallographic Data Centre via www.ccdc.cam.ac.uk/data_request/cif. Supplementary data associated with this article can be found in the online version, at http://dx.doi.org/10.1016/j.jinorgbio.2014.04.002.

References

[1] G.J. Bosl, R.J.N. Motzer, Engl. J. Med. 337 (1997) 242.
[2] E.R. Jamieson, S.J. Lippard, Chem. Rev. 99 (1999) 2467.
[3] P. Abada, S.B. Howell, Metal-Based Drugs 2010 (2012) 1.
[4] C. Marzano, M. Pellei, F. Tisato, C. Santini, Anti Cancer Agents Med. Chem. 9 (2009) 185.
[5] S. Tardito, L. Marchio, Curr. Med. Chem. 16 (2009) 1325.
[6] S. Brem, Cancer Control 6 (1999) 436.
[7] F. Tisato, C. Marzano, M. Porchia, M. Pellei, C. Santini, Med. Res. Rev. 30 (2010) 708.
[8] R.J. Coates, N.S. Weiss, J.R. Daling, R.L. Rettmer, G.R. Warnick, Cancer Res. 49 (1989) 4353.
[9] M. Diez, F.J. Ceda, M. Arroyo, J.L. Balibrea, Cancer 63 (1989) 726.
[10] S.K. Gupta, V.K. Shukla, M.P. Vaidya, S.K. Roy, J. Surg. Oncol. 52 (1993) 172.
[11] G.J. Brewer, Exp. Biol. Med. 226 (2001) 665.
[12] D.S. Sigman, D.R. Graham, V. D'Aurora, A.M. Stern, J. Biol. Chem. 254 (1979) 12269.
[13] R. Alemon-Medina, J.L. Munoz-Sanchez, L. Ruiz-Azurara, I. Gracia-Mora, Toxicology 22 (2008) 710.
[14] A. Riveo-Muller, A. De Vizcaya-Ruiz, N. Plant, L. Ruiz, M. Dobrota, Chem. Biol. Interact. 165 (2007) 189.
[15] M. O'Connor, M.A. Kellett, M. McCann, G. Rosair, M. McNamara, O. Howe, B.S. Creaven, S. McClean, A. Foltyn-Afa, D. O'Shea, M. Devereux, J. Med. Chem. 55 (2012) 1957.
[16] R. Loganathan, S. Ramakrishnan, E. Suresh, A. Riyasdeen, M.A. Akbarsh, M. Palaniandavar, Inorg. Chem. 51 (2012) 5512.
[17] T.K. Goswami, B.V.S.K. Chakravarthi, M. Roy, A.A. Karande, A.R. Chakravarty, Inorg. Chem. 50 (2011) 8452.
[18] A. Prisecaru, M. Devereux, N. Barron, M. Malachy, J. Colleran, A. Casey, V. McKee, A. Kellett, Chem. Commun. 48 (2012) 6906.
[19] J.C. Joyner, J. Reichfield, J.A. Cowan, J. Am. Chem. Soc. 133 (2011) 15613.
[20] T. Kobayashi, S. Tobita, M. Kobayashi, Y. Imajyo, M. Chikira, M. Yashiro, Y. Fugii, J. Inorg. Biochem. 101 (2007) 348.
[21] V. Rajendiran, R. Karthik, M. Palaniandavar, H. Stoeckli-Evans, V.S. Periasamy, M.A. Akbarsha, B.S. Srinag, H. Kishnamurthy, Inorg. Chem. 46 (2007) 8208.
[22] T.W. Hambley, Coord. Chem. Rev. 166 (1997) 181.
[23] K.G. Daniel, P. Gupta, R.H. Harbach, W.C. Guida, Q.P. Dou, Biochem. Pharmacol. 67 (2004) 1139.
[24] A.M. Lozano-Vila, F. Luna-Giles, E. Vinuelas-Zahinos, F.L. Cumbrera, A.L. Ortiz, F.J. Barros-Garcia, A.B.. Rodriguez, Inorg. Chim. Acta 365 (2011) 282.
[25] R. Cejudo, G. Alzuet, M. Gonzales-Alvarez, J.L. Garcia-Gimenez, J. Borras, J.M. Liu-Gonzalez, J. Inorg. Biochem. 100 (2006) 70.
[26] Z.C. Liu, B.D. Wang, B. Li, Q. Wang, Z.Y. Yang, T.R. Li, Y. Li, Eur. J. Med. Chem. 45 (2010) 5353.
[27] Z.C. Liu, B.D. Wang, Z.Y. Ynag, Y. Li, D.D. Qin, T.R. Li, Eur. J. Med. Chem. 44 (2009) 4477.
[28] J. DeRuiter, A.N. Brubaker, W.L. Whitmer, J.L. Stein Jr., J. Med. Chem. 29 (1986) 2024.
[29] C.M. Darby, C.F. Nathan, J. Antimicrob. Chemother. 65 (2010) 1424.
[30] P.C. Dorrestein, H. Zhai, S.V. Taylor, F.W. McLafferty, T.P. Begley, J. Am. Chem. Soc. 126 (2004) 3091.
[31] A. Hazra, A. Chatterjee, T.P. Begley, J. Am. Chem. Soc. 131 (2009) 3225.
[32] R. Schiffmann, A. Neugebauer, C.D. Klein, J. Med. Chem. 49 (2006) 511.
[33] M. Devereux, D. O'Shea, A. Kellett, A.M. McCann, M. Walsh, D. Egan, C. Deegan, K. Kedziora, G. Rosair, H. Muller-Bunz, J. Inorg. Biochem 101 (2007) 881.
[34] M. Devereux, D. O'Shea, M. O'Connor, H. Grehan, G. Connor, M. McCann, G. Rosair, F. Lyng, A. Kellett, M. Walsh, D. Egan, B. Thati, Polyhedron 26 (2007) 4073.
[35] G.M. Sheldrick, Acta Cryst. A64 (2008) 112.
[36] D.S. Raja, N.S.P. Bhuvanesh, K. Natarajan, Inorg. Chem. 50 (2011) 12852.
[37] X. Qiao, Z.Y. Ma, C.Z. Xie, F. Xue, Y.W. Zhang, J.Y. Xu, Z.Y. Qiang, J.S. Lou, G.J. Chen, S.P. Yan, J. Inorg. Biochem. 105 (2011) 728.
[38] L. Cassimeris, J. Morabito, Mol. Biol. Cell 15 (2004) 1580.
[39] M.T. Bogert, B. Naiman, J. Am. Chem. Soc. 57 (1935) 1529.
[40] S. Ratner, H.T. Clarke, J. Am. Chem. Soc. 59 (1937) 200.
[41] F.J. Kreipa, V. Mature, J.J. Finn, J.G. McClarnon, F. Lombardo, J. Am. Chem. Soc. 73 (1951) 1155.
[42] R.C. Elderfield, E.C. McClenachan, J. Am. Chem. Soc. 82 (1960) 1982.
[43] K.S. Ramasamy, R. Bandaru, D. Averett, J. Org. Chem. 65 (2000) 5849.
[44] D.R. Williams, P.D. Lowder, Y.-G. Gu, D.A. Brooks, Tetrahedron Lett. 38 (1997) 331.
[45] V.C. Ezeh, A.K. Patra, T.C. Harrop, Inorg. Chem. 49 (2010) 2586.
[46] L.J. Carlson, J. Welby, K.A. Zebrowski, M.M. Wilk, R. Giroux, N. Ciancio, J.M. Tanski, A. Bradley, L.A. Tyler, Inorg. Chim. Acta 365 (2011) 159.
[47] M.A. Lynn, L.J. Carlson, H. Hwangbo, J.M. Tanski, L.A. Tyler, J. Mol. Struct. 1011 (2012) 81.
[48] S.D. Bella, I. Fragala, I. Ledux, M.A. Diaz-Garcia, T.J. Marks, J. Am. Chem. Soc. 119 (1997) 9550.
[49] W.D. Harrison, D.M. Kennedy, N.J. Ray, R. Sheahan, B.J. Hathaway, J. Chem. Soc. Dalton Trans. (1981) 1556.
[50] P. Nagle, E. O'Sullivan, B.J. Hathaway, E.J. Muller, J. Chem. Soc. Dalton Trans. (1990) 3399.
[51] A.W. Addison, T.N. Rao, J. Reedijk, J. van Rijn, G.C. Vershoor, J. Chem. Soc. Dalton Trans. (1984) 1349.
[52] D. Reinen, M. Atanasov, Chem. Phys. 136 (1989) 27.
[53] S. Roy, P. Mitra, A.K. Patra, Inorg. Chim. Acta 370 (2011) 247.
[54] L.N. Rusere, T. Shalumova, J.M. Tanski, L.A. Tyler, Polyhedron 28 (2009) 3804.
[55] T.C. Harrop, M.M. Olmstead, P.K. Mascharak, J. Am. Chem. Soc. 126 (2004) 14714.
[56] R.E.H.M.B. Osorio, R.A. Peralta, A.J. Bortolzzi, V.R. de Almeida, B. Szpoganicz, F.L. Fischer, H. Terenzi, A.S. Mangrich, K.M. Mantovani, D.E.C. Ferreira, W.R. Rocha, W. Haase, Z. Tomkowicz, A. dos Anjos, A. Neves, Inorg. Chem. 51 (2012) 1569.
[57] A. Neves, L.M. Rossi, I. Vencato, V. Drago, W. Haase, R. Werner, Inorg. Chim. Acta 281 (1998) 111.
[58] L.N. Rusere, T. Shalumova, J.M. Tanski, L.A. Tyler, Polyhedron 28 (2009) 3804.
[59] P. Bruijnincx, P.J. Sadler, Curr. Opin. Chem. Biol. 12 (2008) 197.
[60] F.J. Meyer-Almes, D. Porschke, Biochem 32 (1993) 4246.
[61] R.F. Pasternack, M. Caccam, B. Keosh, T.A. Stephenson, A.P. Williams, E.J. Gibbs, J. Am. Chem. Soc. 113 (1991) 6835.
[62] M. Cory, D.D. McKee, J. Kagan, D.W. Henry, J.A. Miller, J. Am. Chem. Soc. 107 (1985) 2528.
[63] M. Ganeshpandian, R. Loganathan, S. Ramakrishnan, A. Riyasdeen, M.A. Akbarsha, M. Palaniandavar, Polyhedron 52 (2012) 912.
[64] S. Bhattacharyya, A. Sarkar, S.K. Dey, G.P. Jose, A. Mukherjee, T.K. Sengupta, Dalton Trans. 42 (2013) 11709.
[65] F. Xue, C.Z. Xie, Y.W. Zhang, Z. Qiao, X. Qiao, J.Y. Xu, S.P. Yan, J. Inorg. Biochem. 115 (2012) 78.
[66] S. Ramakrishnan, D. Shakthipriya, E. Suresh, V.S. Periasamy, M.A. Akbarsha, M. Planiandavar, Inorg. Chem. 50 (2011) 6458.